Energy transfer and the 2.8-μm emission of Er^{3+}- and Yb^{3+}-doped low silica content calcium aluminate glasses

D. F. de Sousa, J. A. Sampaio, and L. A. O. Nunes
Instituto de Física de São Carlos Universidade de São Paulo, P.O. Box 369, CEP 13560-970 São Carlos, SP, Brazil

M. L. Baesso, A. C. Bento, and L. C. M. Miranda
Departamento de Física, Universidade Estadual de Maringá CEP, 87020-900 Maringá, PR, Brazil
(Received 29 June 1999; revised manuscript received 7 September 1999)

The 2.8-μm emission of Er^{3+}-doped low silica content calcium aluminate glasses sensitized by Yb^{3+} is investigated using conventional spectroscopy. The experimental data are quantitatively analyzed in terms of the energy transfer among the Yb^{3+} and Er^{3+} ions. The energy transfer rate by dipole-quadrupole mechanism was inferred to be larger than by dipole-dipole mechanism. Using the Dexter model of energy transfer, the microscopic parameters of energy transfer by dipole-dipole mechanism were calculated. It was found that the $Yb^{3+} \rightarrow Er^{3+}$ energy transfer constant is 2.6 times greater than the back-energy transfer.

I. INTRODUCTION

Mid-infrared lasers (2–5 μm) have attracted considerable attention in the past 10 years, particularly for their great potentialities as medical lasers and in remote chemical sensing application.[1,2] These kinds of laser devices operating at 2.8 μm were until recently based upon Er^{3+}-doped crystalline hosts[3] [yttrium aluminum garnet (YAG) and yttrium lithium fluoride (YLF) crystals] and fluoride glasses.[4] The main argument for concentrating the search for 2.8-μm laser emission in nonoxide glasses was because this class of glasses demonstrate relatively low nonradiative transition rates due to their well-known maximum phonon energy of approximately 500 cm^{-1}.

In a recent paper,[5] we reported on the observation of 2.8-μm emission from Er^{3+}- and Yb^{3+}-doped low silica content calcium aluminate (LSCA) glasses. Such observation of the 2.8-μm emission from an oxide glass host was at one time a challenge for researchers in the optical material science area. Low silica calcium aluminate glasses have better optical quality and improved thermomechanical[6,7] and chemical-resistance properties when compared to those of the fluoride glasses. Furthermore, LSCA glasses can also be used in fiber form with great advantage over silica fibers due to their lower scattering and multiphonon losses.[8] The successful observation of the 2.8-μm emission in LSCA glasses rested in two important procedures we have adopted, namely, the fabrication of low silica content samples in a vacuum furnace, and rare-earth oxide doping. The low silica content used in our formulation together with the vacuum melting sample preparation not only ensured improved chemical resistance, but also reduced the OH presence in our LSCA glass samples. As it is well known, the presence of OH radicals plays an important role in enhancing the multiphonon relaxation of the excited states of Er^{3+} ions which, in turn, entails in a severe luminescence quenching. On the other hand, the use of Er^{3+}- and Yb^{3+}-doped (LSCA) glasses envisaged to take advantage of the fact that the Yb^{3+} acts as a sensitizer of the Er^{3+} luminescence. A detailed investigation of such pumping mechanism is presented in this paper. The Dexter model[9] is applied to calculate the energy transfer rates by dipole-dipole coupling. The energy-transfer rate by dipole-quadrupole mechanism was inferred using the Kushida formulation.[10] The obtained results showed that the energy transfer rate by dipole-quadrupole coupling seems to be larger than by dipole-dipole. The predominance of the dipole-quadrupole mechanism against dipole-dipole has also been observed in other studies concerning energy transfer between rare-earth ions.[11–13]

II. EXPERIMENTAL PROCEDURES

Two sets of LSCA glasses were prepared from 99.999% purity powders. One purely Er-doped, and henceforth denoted by x Er, had the following weight (%) composition: $(41-x)\%$ Al_2O_3, 47.4% CaO, 7% SiO_2, 4.1% MgO, and $x\%$ Er_2O_3, $x=0.5$, 1, and 2. The second set of glass samples was a doped set denoted as x Er 2 Yb with the following weight (%) composition: $(41-x)\%$ Al_2O_3, 47.4% CaO, 7% SiO_2, 4.1% MgO, $x\%$ Er_2O_3, 2% Yb_2O_3 with $x=0.5$, 1, 2, 3, and 4. The mixtures were melted at 1500 °C in graphite crucibles under vacuum conditions. After 2 h in the melt, the mixture was cooled down to room temperature. The samples so obtained were cut and polished into 3-mm-thick disks of 10 mm in diameter.

The ultraviolet-visible-near-infrared optical absorption spectra were recorded in a Cary 17 spectrophotometer. The photoluminescence decay curves measurements were performed with a diode laser operating at 0.98 μm and modulated by a mechanical chopper as the excitation source. After being dispersed by the 0.3-m Thermo Jarrel Ash monochromator, the signal was collected by a InAs detector. The collected signal was recorded by a Hewlett Packard 54501A-100 MHz digital oscilloscope. All measurements were done at room temperature.

III. RESULTS

The $^4I_{11/2}$ excited state decay curves were measured for both x Er and x Er 2 Yb samples. The signal was measured in

 ©2000 The American Physical Society

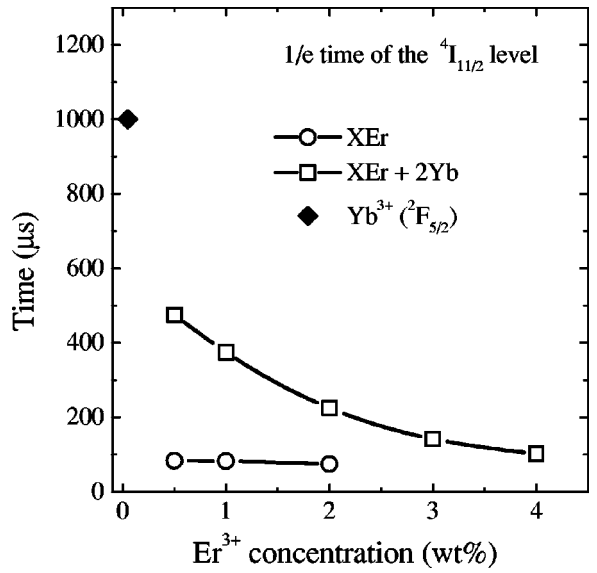

FIG. 1. 1/e time of the $^4I_{11/2}$ level of Er^{3+} corresponding to the $^4I_{11/2} \rightarrow {}^4I_{13/2}$ transition. The lifetime of the $^2F_{5/2}$ level is also included for comparison.

the $^4I_{11/2} \rightarrow {}^4I_{13/2}$ transition (around 2.8 μm) in order to avoid the Yb^{3+} luminescence ($^2F_{5/2} \rightarrow {}^2F_{7/2}$ transition). From the curves the 1/e time (τ) was evaluated which is the time interval where the signal drops to 1/e of its initial value and the results are shown in Fig. 1. Other criteria have been used to evaluate a number representing a nonexponential decay curve. Inokuti and Hirayama[14] have proposed a mean time (τ_m) defined by

$$\tau_m = \frac{\int_0^\infty I(t)dt}{I(0)} \tag{1}$$

where $I(t)$ is the decay curve and $I(0)$ is its initial intensity. As a large discrepancy between the two criteria was not found, we have adopted the 1/e time due to its simplicity. For the x Er samples, where the decay curves are exponentials, the 1/e time is identical to the $^4I_{11/2}$ lifetime and approximately 85 μs. The decay curves of the $^2F_{5/2}$ level was also monitored (observing the luminescence intensity above 1.0 μm where the Er^{3+} no longer emits). Since the Yb^{3+} ions are initially excited, the Yb^{3+} decay rate is found to decrease to a limiting rate, while the Er^{3+} emission rate is seen to increase to the same limiting value, as the Er^{3+} and Yb^{3+} emissions come into equilibrium with each other. Also shown in Fig. 1 is the $^2F_{5/2}$ lifetime measured in a single Yb^{3+}-doped sample, which is about 1.0 ms. For the doped samples, the results clearly show that the effect of the Yb^{3+} ions is to increase the 1/e time of the $^4I_{11/2}$ decay curve. This indicates that the $Yb^{3+} \rightarrow Er^{3+}$ energy transfer may indeed be considered as an efficient pumping channel for the erbium $^4I_{11/2}$ level in our LSCA glass samples.

IV. DISCUSSION

The observed luminescence at 2.8 μm in the single Er^{3+}-doped and Yb^{3+}- and Er^{3+}-doped samples is essentially due to the formulation and fabrication procedures we have used.[5] The low silica content as well as the vacuum melting procedure inhibited the formation of OH radicals in our samples, as manifested by the absence of the characteristic strong absorption bands of these radicals in our spectra. As discussed by Hehlen *et al.*,[17] the presence of OH radicals induces an enhancement of the multiphonon assisted transitions of the Er^{3+} ions, and consequently a quenching of their luminescence. On the other hand, the enhancement of the 2.8-μm luminescence in the doped samples was attributed to a sensitizer role played by the Yb^{3+} ions in those samples. To check whether this view is a reasonable qualitative explanation of the above findings, we present a quantitative analysis of the $Yb^{3+} \rightarrow Er^{3+}$ energy transfer. To this end, we assume the Dexter model[9] describing the energy transfer. According to this model, the energy transfer rate between two ions can occur via a multipolar interaction. In a first approximation, it will be assumed that the dipole-dipole mechanism is predominant over the dipole-quadrupole and quadrupole-quadrupole interactions. The energy transfer rate due to dipole-dipole interaction is given by

$$P_{s\rightarrow a}^{dd} = \frac{3\hbar c^2 Q_a Q_s}{4\pi^3 n^2 R^6} \int \frac{f_s(E) f_a(E)}{E^2} dE, \tag{2}$$

here, $R=(3/4\pi N)^{1/3}$ is the average distance between sensitizer and activator, N is the concentration of absorbing centers, Q_s (Q_a) is the area under the absorption cross section of the sensitizer (activator), f_s (f_a) is the normalized sensitizer (activator) absorption line-shape function, n is the refractive index, and E is the photon energy.

The other two relevant parameters describing the energy transfer are the energy-transfer constant $C_{s\text{-}a}$, and the critical radius of interaction R_c. For dipole-dipole interaction such parameters are defined as

$$C_{s\rightarrow a}^{dd} = P_{s\rightarrow a}^{dd} R^6 \quad \text{and} \quad R_c^{dd} = (C_{s\rightarrow a}^{dd} \tau_s)^{1/6}, \tag{3}$$

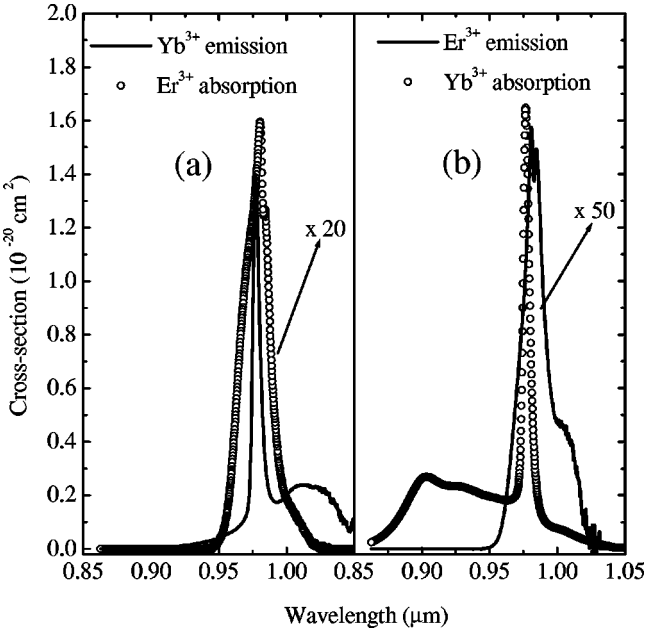

FIG. 2. Sensitizer emission and activator absorption cross sections for the (a) $Yb^{3+} \rightarrow Er^{3+}$ and (b) $Er^{3+} \rightarrow Yb^{3+}$ energy transfer.

TABLE I. Microscopic parameters of energy transfer $C_{s\to a}^{dd}$ and R_c^{dd}, calculated for the doped samples. Q_s and Q_a are the integrated sensitizer emission and activator absorption cross sections in each case.

Sensitizer→Activator	Q_s (cm^2 erg)	Q_a (cm^2 erg)	τ_s (μs)	$C_{s\to a}^{dd}$ (cm^6/s)	R_c (Å)
$Yb^{3+}\to Er^{3+}$	5.03×10^{-34}	3.89×10^{-35}	1100	3.43×10^{-40}	8.37
$Er^{3+}\to Yb^{3+}$	1.65×10^{-35}	7.69×10^{-34}	85	1.32×10^{-40}	4.71

where τ_s is the sensitizer lifetime in a sample without the activator (1.0 ms for Yb^{3+} and 85 μs for Er^{3+}). The critical radius corresponds to the sensitizer-activator distance where the energy transfer and the intrinsic decay of the sensitizer are equally probable. Equation (2) indicates that the energy-transfer rate scales with the square of the dopant concentration. It also follows from Eq. (2) that strong energy transfer results from a good spectral overlap between the sensitizer emission and the activator absorption. The absorption and emission cross sections of the Yb^{3+} and Er^{3+}, as obtained from the experimental data, are shown in Fig. 2. Using these cross sections, together with the corresponding values of τ_s, we have calculated the $Yb^{3+}\leftrightarrow Er^{3+}$ energy transfer parameters. The results for the energy-transfer constant and the critical radius are presented in Table I; it can be seen that the energy-transfer constant for the $Yb^{3+}\to Er^{3+}$ process is 2.6 times greater than that of the $Er^{3+}\to Yb^{3+}$ energy transfer. These results along with the τ values plotted in Fig. 1 corroborate our previous assumption that the energy transfer is more efficient from Yb^{3+} to Er^{3+} than in the opposite sense. Assuming that the net energy transfer will be from Yb^{3+} to Er^{3+}, a macroscopic energy transfer rate $P'_{\mathrm{Yb}\to\mathrm{Er}}$, for the x Er 2 Yb samples can be obtained as follows:[15]

$$P'_{\mathrm{Yb}\to\mathrm{Er}}=\frac{1}{\tau}-\frac{1}{\tau_s}, \tag{4}$$

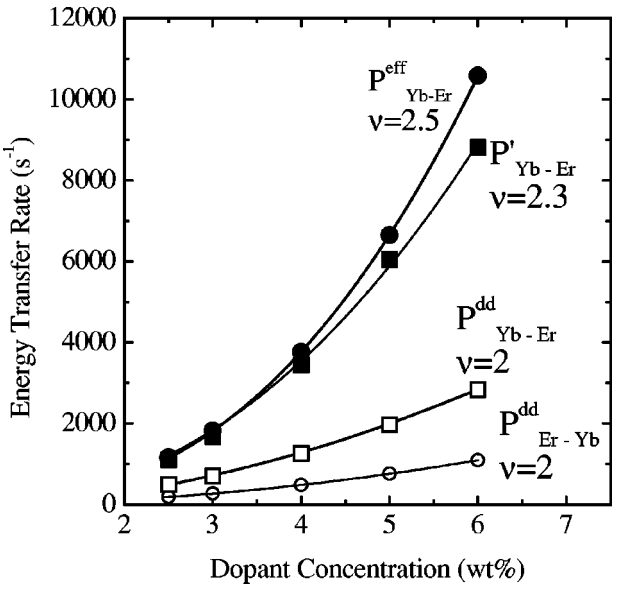

FIG. 3. Energy-transfer rates as a function of the dopant concentration for our x Er 2 Yb low silica calcium aluminate glasses. The open symbols indicate the calculated energy transfer rate by dipole-dipole mechanism. The solid squares represent the macroscopic energy transfer rate obtained from Eq. (4). The solid circles represent the effective value for the energy-transfer rate including the dipole-dipole and dipole quadrupole mechanisms.

where τ is the $1/e$ time of the $^2F_{5/2}$ level in the doped samples, and τ_s is the $^2F_{5/2}$ lifetime measured in a sample without the activator (sample with 0.1 wt% Yb^{3+}). The dependence of the energy-transfer rates in function of the dopant concentration is plotted in Fig. 3. The solid lines in Fig. 3 represent the data fitting to an allometric curve, of the form Ax^{ν}, where x means the total dopant concentration. The open symbols represent the calculated energy-transfer rates by dipole-dipole mechanism, and the solid squares represent the macroscopic energy-transfer rate obtained from Eq. (4). The results of the data fitting of the energy-transfer rates to a function of the type Ax^{ν} shown in Fig. 3, yielded an exponent equal to 2 for the $P_{\mathrm{Yb}\leftrightarrow\mathrm{Er}}^{dd}$ rates, whereas for $P'_{\mathrm{Yb}\to\mathrm{Er}}$ the exponent was found to be equal to 2.3. There are some comments to be made related to the difference between the values of $P_{\mathrm{Yb}\leftrightarrow\mathrm{Er}}^{dd}$ and $P'_{\mathrm{Yb}\leftrightarrow\mathrm{Er}}$. The first point is that it is difficult to compare their absolute values because of the way the two numbers are achieved. $P_{\mathrm{Yb}\leftrightarrow\mathrm{Er}}^{dd}$ is calculated taking into account only two-ion interaction and a single energy-transfer channel; also, the distance R used in Eq. (2) is only a rough approximation of the real case. In contrast, the macroscopic energy-transfer rate $P'_{\mathrm{Yb}\to\mathrm{Er}}$ as defined in Eq. (4) is rigorously valid only if the decays are exponential and it represents a net value considering the average distribution of ions within the material as well as all possible energy-transfer channels. The faster growth of $P'_{\mathrm{Yb}\to\mathrm{Er}}$ with the dopant concentration is the more important point to be treated here. It suggests that other phenomena are occurring in the system. Among the several possibilities to explain such a behavior, we mention that (a) more than two ion processes may indeed

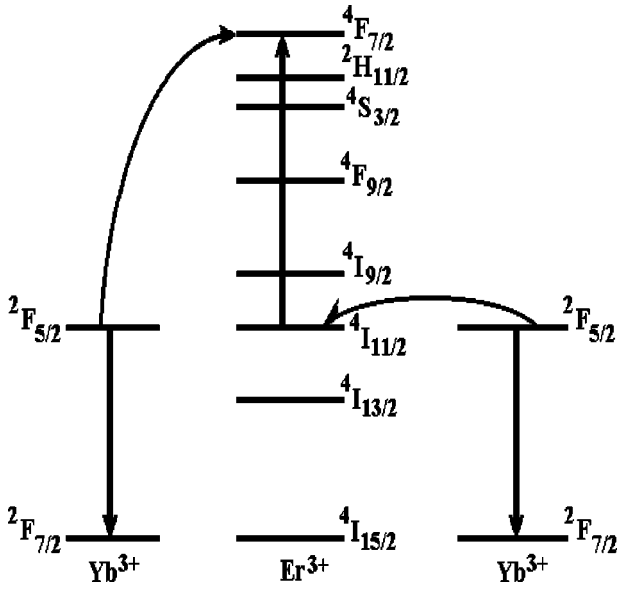

FIG. 4. Energy levels diagram of Er^{3+} and Yb^{3+} showing possible energy-transfer mechanisms leading to upconversion.

TABLE II. Average distance between the ions R, microscopic energy-transfer rates $P^{dd}_{s\to a}$ and $P^{dq}_{s\to a}$, macroscopic energy transfer rate $P'_{s\to a}$, and effective energy transfer rate $P^{eff}_{s\to a}$ obtained for the x Er 2 Yb samples.

x Er 2 Yb	R(Å)	$P^{dd}_{\mathrm{Er}\to\mathrm{Yb}}$ (s^{-1})	$P^{dd}_{\mathrm{Yb}\to\mathrm{Er}}$ (s^{-1})	$P'_{\mathrm{Yb}\to\mathrm{Er}}$ (s^{-1})	$P^{dq}_{\mathrm{Yb}\to\mathrm{Er}}$ (s^{-1})	$P^{dq}_{\mathrm{Er}\to\mathrm{Yb}}$ (s^{-1})	$P^{eff}_{\mathrm{Yb}\to\mathrm{Er}}$ (s^{-1})
$x=0.5$	9.41	190	494	1105	1072	215	1161
$x=1$	8.86	273	709	1667	1736	348	1824
$x=2$	8.05	486	1260	3444	3738	748	3764
$x=3$	7.47	761	1973	6042	6797	1361	6648
$x=4$	7.03	1095	2841	8804	11 050	2213	10 583

contribute to the energy transfer, (b) higher-order multipolar interactions (such as dipole-quadrupole) can be occurring, and (c) clusters form in the sample. The former assumption states that besides the single-step energy-transfer process $^2F_{5/2}$, $^4I_{15/2}\to{}^2F_{7/2}$, $^4I_{11/2}$ leading to the 2.8-μm emission, other higher-order processes may be competing. Due to the high Yb^{3+} absorption cross section, it is very likely that a cooperative energy transfer in which two Yb^{3+} ions simultaneously transfer their energy to an Er^{3+} ion is also a contribution (Fig. 4). In this case, the Er^{3+} undergoes an upconversion to its $^4F_{7/2}$ excited state by means of the cross relaxation $^2F_{5/2}$, $^2F_{5/2}$, $^4I_{15/2}\to{}^2F_{7/2}$, $^2F_{7/2}$, $^4F_{7/2}$.[16] Since this process involves basically three ions, one would expect that, when adding up all these mechanisms, the energy-transfer rate should exhibit a dependence on the dopant concentration between the quadratic and the cubic types. The above explanation can elucidate the origin of the exponent $\nu=2.3$ for $P'_{\mathrm{Yb}\to\mathrm{Er}}$, but the upconverted emission in our samples is extremely weak when compared with the infrared emissions, and we believe it is not sufficient to explain the results. The second hypothesis takes into account higher-order multipolar interactions. According to Dexter, for a completely allowed electric dipole transition, the ratio between $P^{dd}_{s\to a}/P^{dq}_{s\to a}$ is of the order $(a_0/R)^{-2}$, where a_0 is the atomic radius. On the other hand, rare-earth ions are known to present only partially allowed electric dipole transitions. Additionally, the $^4I_{11/2}\to{}^4I_{15/2}$ and $^2F_{5/2}\to{}^2F_{7/2}$ transitions are allowed by an electric quadrupole mechanism. Some reported experiments[18–21] have shown that, in such cases, sometimes the energy transfer by dipole-quadrupole mechanism is of the same order or higher than by the dipole-dipole mechanism. Kushida[10] theoretically treated the situation of energy transfer between rare-earth ions in crystals and calculated the energy-transfer rates for the interaction between two Yb^{3+} ions in YF_3. The results confirmed that the strength of the energy transfer by dipole-quadrupole is larger than by dipole-dipole and were in good agreement with experiments. Using the relation $C^{dd}_{s\to a}/C^{dq}_{s\to a}=5\times10^{13}$ cm^{-2} obtained in Ref. 10, we inferred the value of $P^{dq}_{\mathrm{Yb}\to\mathrm{Er}}$ and $P^{dq}_{\mathrm{Er}\to\mathrm{Yb}}$. The results are in Table II. An effective value for the energy-transfer rate can be defined as $P^{eff}_{\mathrm{Yb}\to\mathrm{Er}}=P^{dd}_{\mathrm{Yb}\to\mathrm{Er}}+P^{dq}_{\mathrm{Yb}\to\mathrm{Er}}-P^{dd}_{\mathrm{Er}\to\mathrm{Yb}}-P^{dq}_{\mathrm{Er}\to\mathrm{Yb}}$. These numbers are in the last column of Table II. Also plotted in Fig. 3 are the values of $P^{eff}_{\mathrm{Yb}\to\mathrm{Er}}$ (solid circles). It can be noted there is a good agreement between the latter data and $P'_{\mathrm{Yb}\to\mathrm{Er}}$. Due to the rough approximation made to obtain $P^{dq}_{\mathrm{Yb}\to\mathrm{Er}}$ and $P^{dq}_{\mathrm{Er}\to\mathrm{Yb}}$, the good agreement between $P'_{\mathrm{Yb}\leftrightarrow\mathrm{Er}}$ and $P^{eff}_{\mathrm{Yb}\leftrightarrow\mathrm{Er}}$ is not important and can be fortuitous. The main point is the exponent ν obtained for $P^{eff}_{\mathrm{Yb}\leftrightarrow\mathrm{Er}}$ in function of the dopant concentration. It is worth noting that the direct evaluation of the energy-transfer rate by dipole-quadrupole mechanism using the Dexter model is a very difficult task, due to the lack of knowledge of the activator absorption cross section by electric quadrupole mechanism. The latter assumption takes into consideration the clusters formation in the sample. The presence of clusters will cause a real energy transfer larger than the expected one, but it is also expected that its value should be concentration independent, which is not verified in our samples.

Knowing P_{s-a} as well as the sensitizer lifetime τ_s measured in a sample without the activator, the efficiency of energy transfer η, as defined by Dexter,[9] is estimated from

$$\eta=\frac{P_{s\to a}\tau_s}{1+P_{s\to a}\tau_s}. \tag{5}$$

The energy-transfer efficiencies are shown in Table III and plotted in Fig. 5 in function of Er^{3+} concentration. It was used in the summation $P^{dd}_{s\to a}+P^{dq}_{s\to a}$ to evaluate Eq. (5) in each case. As can be seen, the energy-transfer efficiency is reaching an upper bound for the x Er 2 Yb samples, but the same statement is not true for the xEr samples. This is due to the relation between $P_{s\text{-}a}$ and τ_s in each case, as suggested by Eq. (5). The data of the energy-transfer efficiencies for the x Er 2 Yb samples were fitted with an exponentially rising function of the type

$$\eta=\eta_0(1-e^{-x/x_0}), \tag{6}$$

where x denotes the Er^{3+} concentration, η_0 and x_0 are fit parameters, and η_0 is the upper limit of the energy-transfer efficiency. From the fit, it was found that $\eta_0=86\%$. In fact, our previous[5] data on the 2.8-μm photoluminescence intensity as a function of the Er^{3+} concentration exhibited a

TABLE III. Efficiencies of the $Yb^{3+}\to Er^{3+}$ and $Er^{3+}\to Yb^{3+}$ energy transfer calculated using Eq. (6). It was used in the summation $P^{dd}_{s\to a}+P^{dq}_{s\to a}$ for the calculation of the efficiencies in each case.

x Er 2 Yb	$\eta_{\mathrm{Er}\to\mathrm{Yb}}$(%)	$\eta_{\mathrm{Yb}\to\mathrm{Er}}$(%)
$x=0.5$	3	53
$x=1$	5	64
$x=2$	9	78
$x=3$	15	86
$x=4$	22	91

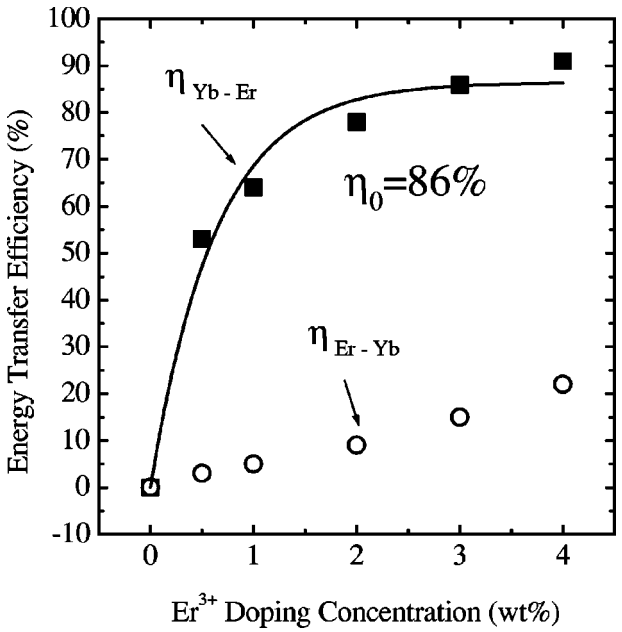

FIG. 5. Energy-transfer efficiency as a function of the Er^{3+}-doping concentration for our *x* Er 2 Yb low silica calcium aluminate glasses. The solid squares indicate the Yb^{3+}-Er^{3+} energy-transfer efficiency, and the open circles represent the Er^{3+}-Yb^{3+} energy-transfer efficiency. The solid line is a fit to Eq. (6).

quenching for Er^{3+} concentration above 4 wt %. This upper bound for the energy-transfer efficiency may be due to the fact that at elevated Er^{3+} concentrations, other energy-transfer processes such as energy migration and upconversion can become important, leading to additional losses.

V. CONCLUSION

We have reported on the $Er^{3+} \rightarrow Yb^{3+}$ energy transfer in LSCA glasses. The experimental data of the Yb^{3+} absorption and Er^{3+} emission cross sections exhibited a good spectral overlap with the result that an efficient $Yb^{3+} \rightarrow Er^{3+}$ energy transfer sets in. The energy transfer between the Yb^{3+} and Er^{3+} ions was quantitatively analyzed using the Dexter model. It was found that, while excitation energy is transferred in both directions, the energy-transfer constant for the $Yb^{3+} \rightarrow Er^{3+}$ process is 2.6 times greater than the back-energy transfer by dipole-dipole mechanism. This confirmed our previous hypothesis[5] that an efficient energy transfer from Yb^{3+} to Er^{3+} is the dominant mechanism responsible for the observation of the 2.8-μm emission from these low silica content aluminate glasses.

The discrepancy between the microscopic and the macroscopic energy-transfer rates was tentatively explained by the addition of the energy transfer by dipole-quadrupole mechanisms, as this latter process has dependence $\frac{8}{3}$ upon dopant concentration and a strength greater than the dipole-dipole coupling for rare-earth ions. Another possible explanation is the addition of the cross relaxation that leads to the upconverted luminescence of the Er^{3+}. We think that the cooperative energy transfer is also occurring but it is so weak and cannot explain the discrepancy. In the above analysis, it has to be borne in mind that the obtained values for the macroscopic energy transfer are approximations due to the use of Eq. (4), which is rigorously true only when the decays are exponentials. On the other hand, the most important feature is the faster growth of Eq. (4) in function of dopant concentration and not its absolute value.

Finally, it should be mentioned that our findings for the 2.8-μm emission in these LSCA glasses contrast with those reported by Zou and Izumitani[22] in the case of the 1.54-μm emission in different aluminate glasses. For their Er^{3+}-doped aluminate glasses sensitized by Yb^{3+}, these authors have found that the back-energy transfer is much more efficient than the Yb^{3+} to Er^{3+} energy transfer. They have then Er^{3+}-doped aluminate glass sensitized by Yb^{3+} as not a good candidate for infrared erbium laser glass.

[1] R. M. Dwyer and M. Bass, in *Lasers in Medicine*, edited by M. Ross (Academic, New York, 1977), Vol. 3, p. 107, and references therein.
[2] K. Kincade, Laser Focus World **32**, 73 (1996).
[3] G. J. Kintz, R. Allen, and L. Esterowitz, Appl. Phys. Lett. **50**, 1553 (1987).
[4] S. A. Pollack and M. Robinson, Electron. Lett. **24**, 320 (1988).
[5] D. F. de Sousa, L. F. C. Zonetti, M. J. V. Bell, J. A. Sampaio, L. A. O. Nunes, M. L. Baesso, A. C. Bento, and L. C. M. Miranda, Appl. Phys. Lett. **74**, 908 (1999).
[6] J. E. Shelby, J. Am. Ceram. Soc. **68**, 155 (1985).
[7] M. L. Baesso, A. C. Bento, A. R. Duarte, A. M. Neto, L. C. M. Miranda, J. A. Sampaio, T. Catunda, S. Gama, and F. C. G. Gandra, J. Appl. Phys. **85**, 8112 (1999).
[8] M. E. Lines, J. B. MacChesney, K. B. Lyons, A. J. Bruce, A. E. Miller, and K. Nassau, J. Non-Cryst. Solids **107**, 251 (1989).
[9] D. L. Dexter, J. Chem. Phys. **21**, 836 (1953).
[10] T. Kushida, J. Phys. Soc. Jpn. **34**, 1318 (1973).
[11] T. T. Basiev, Yu. V. Orlovskii, and Yu. S. Privis, J. Lumin. **69**, 187 (1996).
[12] K. Tonooka, K. Yamada, N. Kamata, and F. Maruyama, J. Lumin. **60&61**, 864 (1994).
[13] I. R. Martín, V. D. Rodriguez-Mendoza, V. Lavín, E. Montoya, and D. Jacque, J. Chem. Phys. **111**, 1191 (1999).
[14] M. Inokuti and F. Hirayama, J. Chem. Phys. **43**, 1978 (1965).
[15] M. Malinowski, Z. Frukacz, M. F. Joubert, and B. Jacquier, J. Lumin. **75**, 333 (1997).
[16] F. E. Auzel, C. R. Acad. Sci. **262**, 1016 (1966).
[17] M. P. Hehlen, N. J. Crockcroft, T. R. Grosnell, and A. J. Bruce, Phys. Rev. B **56**, 9302 (1997).
[18] J. D. Axe and P. F. Weller, J. Chem. Phys. **40**, 3066 (1964).
[19] L. G. Van Uitert and L. F. Johnson, J. Chem. Phys. **44**, 3514 (1966).
[20] L. G. Van Uitert, E. F. Dearborn, and J. J. Rubin, J. Chem. Phys. **45**, 1578 (1966).
[21] E. Nakazawa and S. Shionoya, J. Chem. Phys. **47**, 3211 (1967).
[22] X. Zou and T. Izumitani, J. Ceram. Soc. Jpn. **101**, 85 (1993).